ADVANCED MATERIALS TECHNOLOGIES
www.advmattechnol.de

Mechanically Stable PMMA-Based Large-Area Nano-Channels with Sub-10 nm Depth

Min Liu, Tobias Reimer, Yongkang Wang, Mathias Kläui, Yaowen Xing, Xiahui Gui, Yijun Cao, Rüdiger Berger, Hai Wang, and Mischa Bonn**

Artificial sub-microfluidic and nanofluidic devices allow for studying mass or ion transport effects under spatial confinement. It remains challenging to fabricate large-scale, nanofluidic channels of well-defined thickness for fundamental studies and practical applications, especially for extreme confinement conditions (e.g., with sub-10 nm channel height). Here, a strategy is reported to fabricate large-scale nano-channels with the channel height down to 5.0 nm. The fabrication is enabled by developing ultra-flat and ultra-thin polymethylmethaacrylate (PMMA) layers as the spacer. The ease of scaling up the channel length to a millimeter in the lateral dimensions with high mechanical stability is demonstrated. Furthermore, experimental evidence is provided of the role of the mechanical coupling between the spacer and capping materials in determining the device's mechanical properties, and how controlling the channel width and the top graphite thickness can be employed to tailor the device's mechanical properties. Finally, employing near-field IR experiments, the decay constant is established for the near-field absorption intensity of PMMA molecules inside the channel by increasing the top layer thickness. This work develops a novel method for fabricating large-area, mechanically stable nano-channels for nanofluidic devices and lays the foundation for further in situ spectroscopic studies of electrochemistry within sub-10 nm confinement.

1. Introduction

In recent decades, phenomena associated with the confinement of molecules and ions have attracted increasing attention in many research fields,[1] including electrochemical supercapacitors,[2] membranes,[3] and sensors,[4] etc.[5,6] where mass or ion transport in the porous or slit materials plays an important role in dictating the device performance. A few recent examples include: 1) Tunuguntla et al. reported a confinement-enhanced proton transport effect, in which proton conductivity in carbon nanotubes with sub-nm diameter exceeds that in bulk water by an order of magnitude. The authors attributed the effect to the formation of 1D water "wires" following the Grotthuss mechanism.[7] 2) Electrolytes under 1- or 2D confinement have been shown to host many fascinating nonlinear ionic transport properties, including the ionic Coulomb blockade effect for ion pumping, and hysteretic conductions of ions relevant to memristor applications.[8–10] 3) Under extreme sub-10.0 nanometer confinement, water molecules have been shown to be dielectrically inactive in the thickness direction with a substantially lower dielectric constant than the bulk.[11]

Understanding how the nanoscale confinement impacts the liquid mass transport or ionic charge flow is mandatory in

M. Liu
School of Chemical Engineering and Technology
China University of Mining and Technology
Xuzhou, Jiangsu 221116, China

M. Liu, Y. Wang, H. Wang, M. Bonn
Molecular Spectroscopy Department
Max Planck Institute for Polymer Research
55128 Mainz, Germany
E-mail: h.wang5@uu.nl; bonn@mpip-mainz.mpg.de

The ORCID identification number(s) for the author(s) of this article can be found under https://doi.org/10.1002/admt.202401172

DOI: 10.1002/admt.202401172

M. Liu, Y. Xing, X. Gui, Y. Cao
State Key Laboratory of Coking Coal Resources Green Exploitation
China University of Mining and Technology
Xuzhou, Jiangsu 221116, China

T. Reimer, M. Kläui
Institute for Physics
Johannes Gutenberg University Mainz
55099 Mainz, Germany

T. Reimer, M. Kläui
Graduate School of Excellence Materials Science in Mainz
Staudinger Weg 9, 55128 Mainz, Germany

R. Berger
Physics of Interfaces Department
Max Planck Institute for Polymer Research
55128 Mainz, Germany

H. Wang
Nanophotonics
Debye Institute for Nanomaterials Science
Utrecht University
Princetonplein 1, Utrecht 3584 CC, The Netherlands

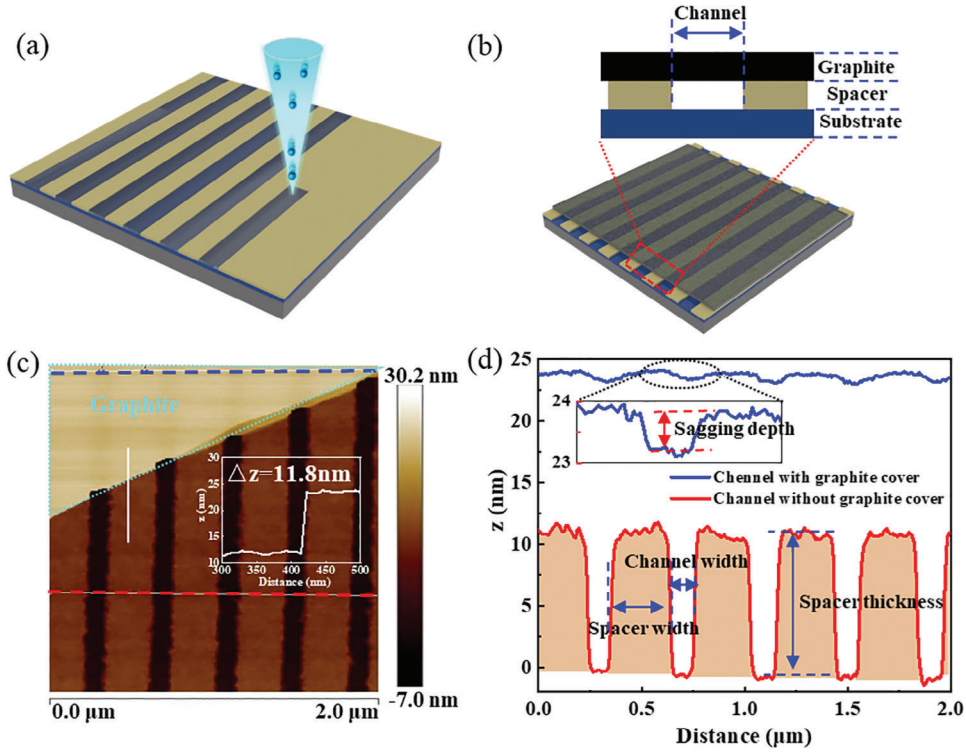

Figure 1. The fabrication and characterizations of 2D-material-based nano-channels. a) Schematic of the fabrication of nanometer-thick homogeneous PMMA patterns by electron beam lithography. (gray for silicon, blue for silica layer, and yellow for PMMA spacers). b) Schematics of graphite-covered nano-channels. c) The topography on the edge of the graphite-flake-covered nano-channels using a PMMA spacer. Red and blue dashed lines show the line scans shown in (d). d) Profiles along the dashed lines in Figure (c). The red dashed line shows the section of the uncapped nano-channel; the blue line is the height measurement on the graphite.

the above examples. Technical developments in reliable, large-scale artificial nanoscale ion channels are required.[12] Currently, there are three main categories of nano-channel developed for studying the ion or liquid confinement effects spanning from zero to 2D geometries: 0D solid-state nano-pore,[13] 1D carbon nanotubes,[14] and 2D atomic-scale ion channels based on van der Waals (vdW) materials.[15] Among them, 2D ion channels rely on defining an atomically precise 2D spacer using vdW layers with controllable layer numbers,[16–19] which revolutionize and bring the fluidic physics down to sub-nanometers, and even single-molecule scale. While these artificial 2D ion channels provide an excellent platform for fundamental research, their lateral size is limited to tens of micrometers because of the small size of the exfoliated thin 2D crystal.[20] Devices with a thickness of a few nanometres but covering lateral length scales up to millimeters have great potential for nanoionics applications (e.g., sensory and information storage) and further allow for integration of spectroscopies for and investigating ionic interactions under confinement.[21,22] In this direction, polymethylmethacrylate (PMMA) combined with electron beam lithography (EBL) has been shown to have great potential for large-area channels with sub-10.0 nm height.[23,24] Although it remains challenging to achieve ≈sub-nm scale confinement enabled by vdW channels, the scalability of the "polymer-based" soft 2D channels is appealing for further device integration and in situ spectroscopic studies.

Besides challenges in achieving spatial confinement, questions remain about the mechanical stability of nanofluidic devices, which is important for both fundamental studies and applications. Previous studies based on vdW-based spacers have shown notable sagging,[12] causing the channel thickness to be reduced in the center compared to the edges. A detailed understanding of the parameters controlling the sagging and the mechanical strength of nanoscale channels is thus desirable for further developing large-scale, well-defined channels under strong spatial confinement.

This study combines PMMA spacers with graphite top layers to fabricate lateral-area nanodevices with a sub-ten nanometer height. We explore the role of mechanical interactions between the PMMA and graphite layers in determining channel stability. The key idea for our channel fabrication lies in employing nanometer-thin ultra-flat PMMA films as the channel spacer developed by EBL. Subsequently, the large-area channel is covered with graphite flakes with varied thicknesses. We demonstrate 2D nanodevices with heights of down to 5.0 nm and lateral dimensions of up to hundreds of micrometers. Furthermore, we investigate the mechanical stability of nanodevices with/without external load and unveil the critical role of mechanical interactions between the spacer and the capping layer in enhancing their mechanical strength. Finally, we employ scanning force microscopy-based infrared spectroscopy (SFM-IR) to explore the shielding rate of top-layer graphite to near-field infrared feedback. Our

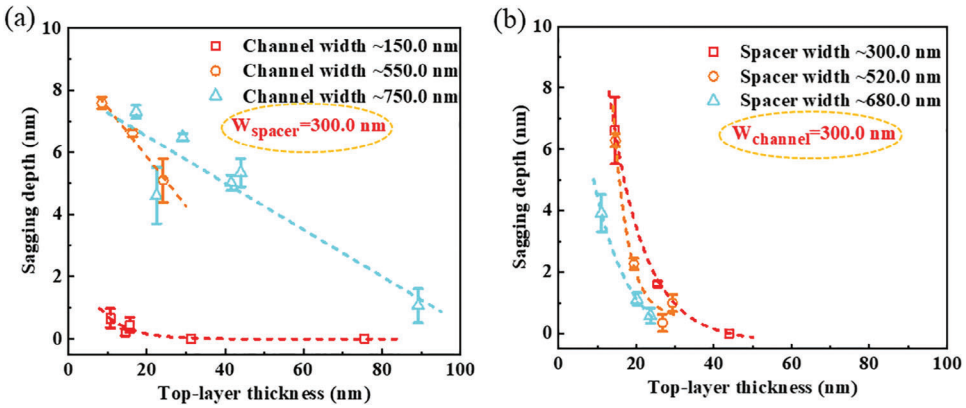

Figure 2. Mechanical stability of 13.0 nm graphite-capped nano-channels. a) The role of top-layer thicknesses and channel width in controlling the sagging depth. The studies are based on devices with a fixed spacer width of 300.0 nm, and a channel height of 13.0 nm. b) The impact of top-layer thicknesses and spacer width in tuning the sagging depth. The studies are based on devices with a fixed channel width of 300.0 nm, and a channel height of 13.0 nm.

work thus develops a new method to fabricate scalable and mechanically stable artificial nano-channels with sub-ten nanometer channel heights.

2. Results and Discussion

2.1. Nano-Channel Fabrication with PMMA Spacer

Inspired by previous studies, our concept relies on developing and employing a flat, nanometer-thin polymer layer as the spacer instead of a 2D material.[15] The spacer layer is prepared by spin-coating the PMMA onto a silicon wafer and controlling the thickness by finely adjusting the spin rate and PMMA concentration (see details in the Supporting Information). As shown in the exemplary profile of the PMMA film, the surface roughness can be controlled down to a root mean square value of $Rq = 0.26$ nm. Following the PMMA-thin-film preparation, we create the channels by selectively etching PMMA at the area patterned by EBL, as shown in **Figure** 1a. Finally, we cap channels with a mechanically exfoliated graphite flake using a commercial mechanical transfer stage for 2D materials; graphite has been chosen as the model top layer because of its atomically flat surface, good mechanical properties, and common application in nanofluidic devices fabrication, which allows direct comparison whenever needed.[15] Figure 1b shows a schematic of the resulting device. The thickness of the spin-coated PMMA film determines the height of the nano-channel. The small height-to-width ratio of the channel at the nanoscale makes our constructed nanodevices an alternative to vdW-based 2D channels for applications requiring large-area devices.

Figure 1c displays a representative scanning force microscope (SFM) image of our channels across the capping edge, which shows the height differences between the capping top layer graphite, the channels, and the PMMA spacers. Several line profiles are plotted in Figure 1d, from which we can readily determine the channel characteristics (e.g., the channel and spacer width, the spacer thickness) without the top layer. The blue and red profiles correspond to the blue and red dashed lines in Figure 1c. The morphology of capped graphite, shown as the blue curve, is shown in the inset of Figure 1d. From this profile, we determined the sagging depth of the top layer, defined by the height variation between the channel (e.g., no PMMA underneath) and the PMMA spacer area, for example, which is ≈0.7 nm as shown in Figure 1d.[12]

With our method, the height of the nano-channel could be controlled down to ≈5.0 nm, as exemplified in Figure S2 (Supporting Information). The spacer thickness is maintained when the top-layer graphite is present; see the spacer thickness in Figure S3 (Supporting Information) before covering and after graphite removal. The thickness of the film can be flexibly controlled and is uniform over an area of several millimeters across in the center of the spin-coated nanometer-thin film. Thus, this strategy can potentially fabricate millimeter-scale, large-area nanodevices for practical application in the future, see Figure S4 (Supporting Information). It may provide a practical platform for large-scale nanofluidic device applications, complementing methods that are based on typically small-area 2D material platforms.[25]

2.2. The Mechanical Stability of the Top-layer Graphite on Nano-Channel

2.2.1. The Sagging Depth of Near-Free-Standing Graphite Top Layer on Nano-Channel

The mechanical stability of the nano-channel is essential, e.g., for nanofluidic experiments. Here, we investigate the correlation between the sagging depth of the near-free-standing top-layer graphite and the key factors, including the channel width, the spacer width, and the graphite thickness, as shown in **Figure** 2. A small force, as low as 2.0 nN, is applied in the peak force SFM measurement to minimize the impact of the measurements on the vertical bending of the graphite.

For a given channel height, the interplay among the top-layer thickness, the channel width, and the spacer width (see the variables defined in Figure 1d) are expected to have an effect on the channel stability, which we characterize by the sagging depth of the top-layer. First, we explore the interplay between the

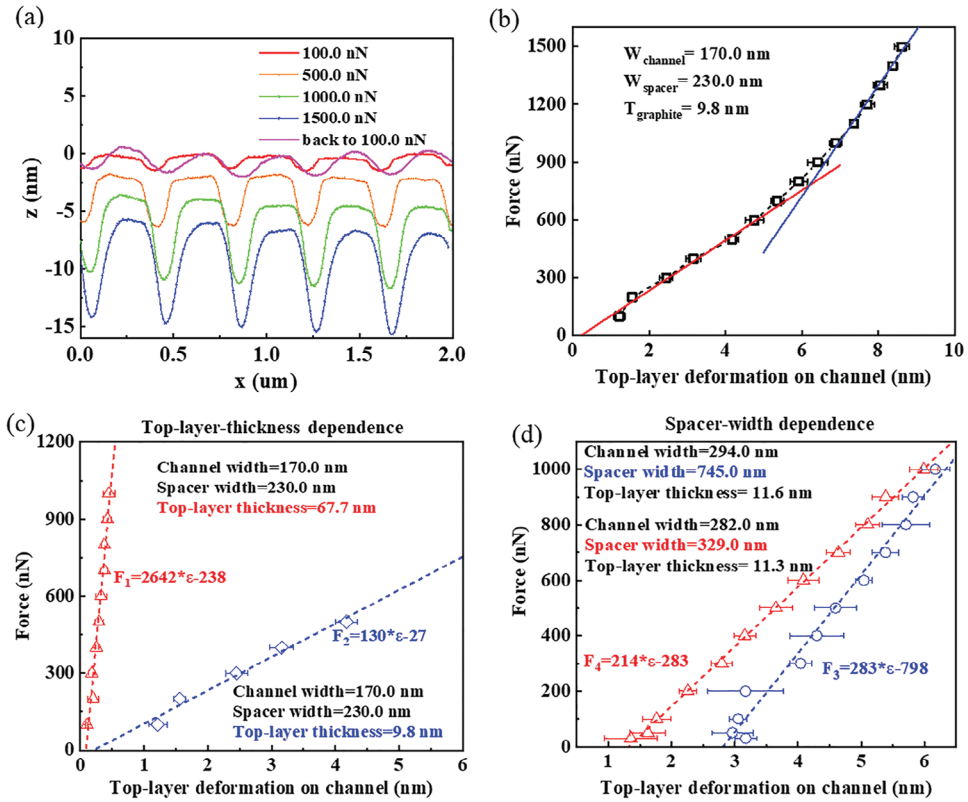

Figure 3. The deformation of the graphite is dependent on the external force applied by the SFM tip. a) Line profiles on graphite under different force loads. b) The correlation between the top-layer graphite deformation on the channel and the applied force. c,d) are the top-layer sagging depth variation with the applied force on nanodevices with varied graphite thicknesses and spacer widths.

top-layer thickness and the channel width with a fixed spacer width (300.0 nm) under 13.0 nm confinement. As shown in Figure 2, the sagging depth decreases with increasing top-layer thickness for a given channel width. This result can be intuitively understood by noting that the mechanical strength of the graphite improves with thickness (which is confirmed by the loading experiments in **Figure 3**). Furthermore, for a fixed graphite capping layer thickness, the sagging depth becomes smaller for narrower channel widths. This observation provides clear evidence of the role of mechanical coupling between the top layer and the PMMA pillars in determining the stiffness and, thus, the mechanical stability of the channels.[26,27] No clear sagging was observed for the narrowest channels (e.g., with a width of 150.0 nm) when the top layer is thicker than 20.0 nm.

Second, we study how the interplay between the top-layer thickness and the channel width (with a fixed channel width of 300.0 nm and spacer thickness of 13.0 nm) impacts mechanical stability. Figure 2b shows that the sagging depth decays exponentially with increasing the graphite thickness for a given channel width. Furthermore, increasing the spacer width drastically lowers the sagging depth for a very thin top-layer thickness. This further supports the role of mechanical coupling between the top-layer and PMMA layers in dictating the channel's mechanical strength. As expected, the effects become weak for a stiff, thick top layer.

Overall, our results unveil that channels with a high ratio between the spacer and channel width, and a thick capping graphite layer enhance the mechanical stability of our channels. The interactions between the top layer and the spacer layer can serve as a critical parameter to tailor the mechanical stability of the 2D channels.

How do our channels compare to other vdW channels with, e.g., graphite as both the spacer and top layer in terms of mechanical stability? For that, we developed PMMA-based channels with characteristics comparable to those using graphite spacers and compared their sagging profiles. As listed in **Table 1**, we can see that while the channel width and the top layer thickness are similar, our channels employ narrower and higher spacers than those of the graphite-spacer-based nano-channels.[14] Even with the latter two unfavorable features, we find a small sagging depth of $\approx 1.4 \pm 0.2$ nm for our PMMA spacers, which is much shallower than that of graphite ones with a sag depth of $\approx 4.8 \pm 0.1$ nm. Again, this comparison consolidates our conclusion on the importance of mechanical interactions between the top layer and spacer layers in strengthening the channel's mechanical properties:, i.e., the adhesion or friction between the PMMA spacer and the graphite top layer likely prevents the top-layer from collapsing.

2.2.2. The Vertical Elasticity of Top-Layer Graphite Under Loading

We further expand the study on the mechanical strength of our devices by applying an external force to the outer surface

Table 1. Comparison of sagging depth with PMMA and graphite as a spacer*).

Spacer	Channel width [nm]	Top layer thickness [nm]	Spacer width [nm]	Spacer thickness [nm]	Sagging depth [nm]
Graphite	560.0	52.0	630.0	5.2	4.8 ± 0.1
PMMA	549.0	61.2	459.0	7.1	1.4 ± 0.2

*) Data for graphite spacer (first row) from reference.[15]

of graphite to mimic the operating conditions under, e.g., hydrostatic pressure. For that, we conduct applied-force-dependent channel deformation characterizations by loading force to the channels by the SFM tip. Figure 3a depicts the traces of the cross-section and the sagging depth of top-layer graphite under various force loadings. The traces of 500.0, 100.0, and 1500.0 nN have been shifted by 2 nm in the *y*-axis for comparison. As shown in Figure 3b, the vertical deformation of the graphite top layer increases linearly with the increasing load. This observation can be rationalized by a previous report, in which the graphene has been shown to bend linearly under a small load based on the mechanical studies of double-edge clamped free-standing graphite and graphene.[26,27] We note that when the load is below 500.0 nN, the top layer could spring back to the initial state after the load is removed, i.e., the sagging is elastic and thus reversible. However, when the external load exceeds 500.0 nN, as shown in Figure 3a, the slope of the force-deformation curve increases substantially, which likely involves the irreversible deformation of PMMA. This deformation cannot fully recover even when the external load is withdrawn. This results in the sag of graphite being unable to be reset, as shown in Figure S6 (Supporting Information).

Our vertical elasticity test of the top-layer graphite provides insight into the capability of the graphite on the nano-channel to resist the external load. The slope of the deformation-force curves provides insight into the stiffness of the graphite layers before the occurrence of deformation of the PMMA spacer. The effect of graphite thickness and spacer width on the elasticity is shown in Figure 3c,d. The graphite thicknesses on the channels are 67.7 and 9.8 nm (with 170.0 nm channel width and 230.0 nm spacer width), and the slopes of the curves are 2642 and 130 N m^{-1}, respectively. These quantitative studies confirm that, as expected, the vertical stiffness of graphite increases with its thickness. Interestingly, this increase scales superlinearly with graphite layer thickness: the ratio of the slope and graphite layer thickness is three times larger for the thicker layer. Moreover, Figure 3d reveals that the elasticity of graphite on 745.0 and 329.0 nm wide spacers (with 294.0 and 282.0 nm in channel width, 11.6 and 11.3 nm in the top-layer graphite thickness) is 283.0 and 214.0 N m^{-1}, respectively. The intersections of curves with the *x*-axis in Figure 3c, which represent the sag without loading as discussed in Section 2.2, are ≈0.1 and 0.2 nm, aligning with the result in Figure 2a.

2.3. Imaging of Nanodevice with SFM-IR

We used near-field spectroscopy, SFM-IR to shed light on the local distribution of different materials in the channels.[28] The working principle relies on detecting the local thermal expansion of materials of interest under the SFM tip upon illuminating with near-infrared light.[29] This SFM method allows recording IR-spectra and mapping of the distribution of materials while scanning. We used SFM IR to investigate the PMMA underneath the graphite. Thus, we explore the cleanliness of the prepared channels spectroscopically with nanometer resolution.

Figure 4a shows the IR spectra recorded with the SFM probe on PMMA and in the channel, where 2 and 1 are the probe positions marked in Figure 4b,c. Figure 4b,c show the topography of the graphite uncovered channel and the SFM-IR scanning at 1730 cm^{-1}. We attribute the broadband absorption region from 980–1160 cm^{-1} to the Si–O–Si stretching mode of SiO_2 of the Au-coated probe.[30] The peak at 1266 cm^{-1} is typical for probe contamination during probe storage and transfer in PDMS gel boxes.[31] The peak at 1730 cm^{-1} in the spectra recorded at position 2 is attributed to the C═O stretching of PMMA,[32] which is not observed at position 1 in the channel. The IR scanning results in Figure 4c demonstrate good contrast between the channel and PMMA area, providing direct evidence of the cleanness of channels. The negligible PMMA residuals in the channel region after the fabrication indicate the reliability of the fabrication method.

Finally, we explore how the thickness of the top layer affects the near-field signal of targeted chemical information underneath the nano-channel. For that, we focus on the C═O stretching band of PMMA and investigate how the signal scales with the top layer thickness. Figure 4d shows the C═O stretching band of normalized spectra recorded on bare, monolayer, and 29-layer graphene-covered devices. The 29 graphene layers are deduced by dividing the graphite thickness of 9.8 nm by the monolayer graphene thickness of 0.33 nm.[33] First of all, we observe that the C═O stretching experiences a blueshift from 1731 to 1757 cm^{-1} when it is covered by monolayer graphene. The reason behind this shift in the stretching mode remains unclear and may be caused by the strong van der Waals interaction between the graphite top layer or silica substrate and the PMMA spacer. In **Figure** 4e, we present how the C═O stretching band signal strength (by integrating the spectra area) scales with the graphene layer number, which we further fit by an exponential decay. Based on the fit, we can infer the exponential decay coefficient of 0.16. This indicates a critical graphene layer number of 6–7 (=~1/0.16) or a cut-off thickness of ≈2.0 nm for using PiFM to imagine local chemical information in nanoscale channels covered by graphite.

3. Conclusion and Outlook

In summary, we propose here an efficient and feasible strategy to fabricate the mechanically stable, large area 2D-material-based nanodevice with sub-10 nm channel height feature. We characterize the channel by scanning force microscopy and study the impact of several channel parameters on the mechanical stabilities (sagging of top-layer graphite) with and without external loading. Finally, we conduct the SFM-IR to investigate how the top

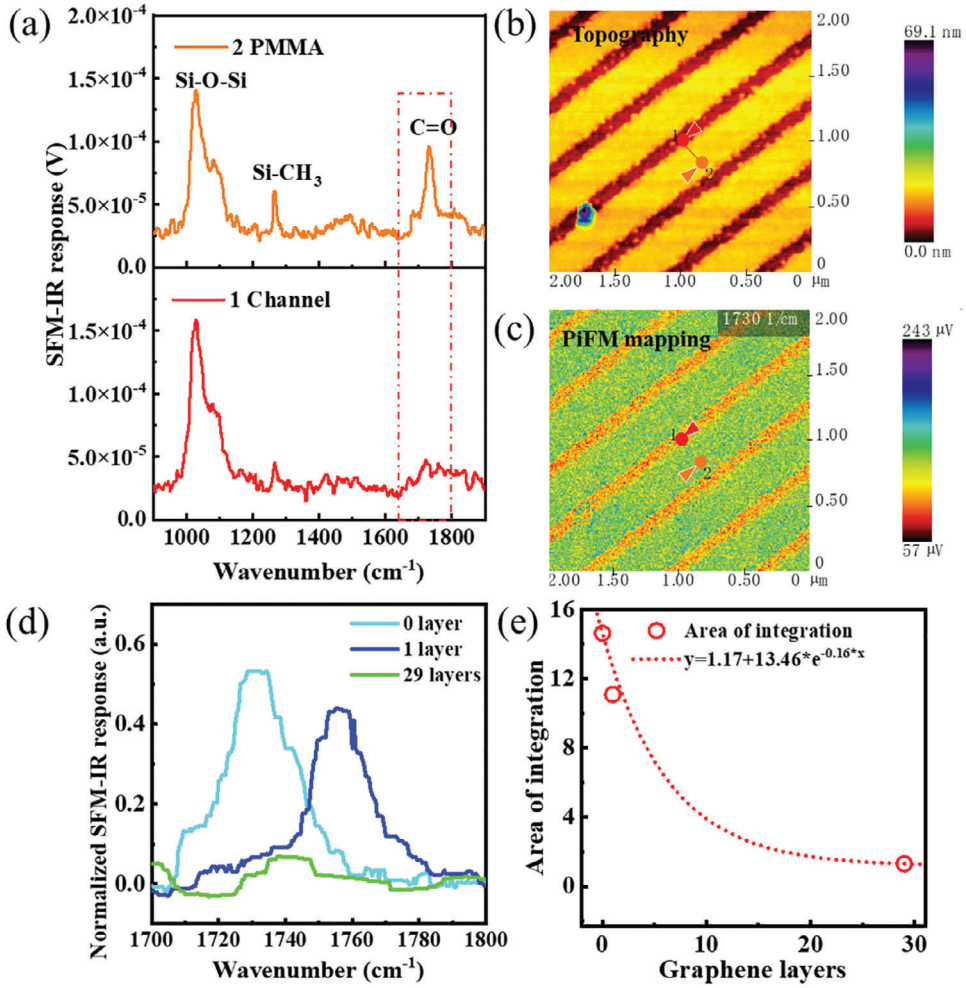

Figure 4. The screening of graphite to near-field IR feedback. a) The PiF spectra on the PMMA spacer and the channel are marked as point 2 and point 1 with triangles in figures (b) and (c). b) The morphology of graphite-uncovered PMMA spacers. c) The PiFM mapping in the same sample position shown in (b). d) The C═O stretching band of normalized PiF spectra recorded on graphene-covered devices. e) The integrated area of (d), tentatively fitted with an exponential function.

layer graphite affects the near-field signal by PiFM. Our study provides important guidelines for the fabrication of large-area nanodevices under sub-10 nm confinement and the key factors for channel stabilization and lays the foundation for further in situ spectroscopic studies of local chemical information in the channels under the sub-10 nm confinement. This strategy also offers a novel approach to studying the transport behavior of ions, molecules, and nanoparticles in nanoconfinement and a new concept to tailor the physical and chemical properties of the capping 2D materials.

4. Experimental Section

Materials and Chemicals: Polymethylmethacrylate (950K MW, PMMA A 11) was purchased from MicroChem. Methylisobutylketone (M.I.B.K., micropure) was purchased from TECHNIC FRANCE. The electron beam lithography developer is M.I.B.K. solution, which was prepared by dissolving in 2-propanol with a volume ratio of 1:4. Silicon wafers were purchased from Si-Mat Silicon Materials. Polydimethylsiloxane (PDMS, SYLGARD 184) was purchased from DOW. CVD-grown graphene was purchased from Grolltex Inc. Flake graphite was purchased from NGS trading & consulting GmbH. The blue tape (BT-150P-LC) was purchased from Nitto. Sulfuric acid (97%), 2-Propanol (≥99.8%), and Acetone (≥99.5%) were purchased from Honeywell. Hydrogen peroxide solution (33% H_2O_2) and ethanol absolute were purchased from VWR Chemicals.

Silicon Wafer Preparation and Graphite Exfoliation: The silicon wafer was cut into small pieces, 1.0 mm wide and 2.0 mm long, and first cleaned with piranha solution (H_2SO_4:H_2O_2 = 7:3 in volume) at 80 °C for 30 min. The wafers were then cleaned with ultrasonic baths subsequently in acetone, ethanol, and Milli-Q water for 5 min, respectively. After blow-drying in nitrogen, oxygen plasma was used to make the surface homogeneously hydrophilic. The graphite flakes were prepared by mechanical exfoliation from natural graphite with blue tape and cured PDMS stamp (9:1 base/curing in weight and stored at room temperature for several days until the mixture was fully cured). First, the blue tape exfoliates the graphite to get a fresh and smooth surface. Then, the blue tape was used to pick up graphite sheets and release them on 1–2 mm thick PDMS. Choosing proper graphite flake on the PDMS with an optical microscope and cutting it down as a stamp for the transfer.

Nano-Channel Preparation: PMMA films were first prepared by spin coating. PMMA was dissolved in Anisole in a series of concentrations ranging from 0.25% to 2%. Spin coating was carried out with a spin rate of 3000 rpm for 1 min with subsequent drying in air. The thickness was

measured using AFM by scanning the edge of the scratch created by a sharp tip. The PMMA-based nano-channel was then fabricated by EBL. The PMMA-coated substrate was baked on the hot plate at 180 °C for 30 s to remove trace amounts of water and Anisole before the EBL. The spin-coating and baking procedures together take approximately four minutes. The acceleration voltage was 3 kV to avoid over-exposure. The structure was developed in methyl isobutyl ketone solution for 10 s and followed with 30 s of 2-Propanol washing. An exemplary image of developed PMMA channels with 5 nm channel height is shown in Figure S2 (Supporting Information). The preparation of the nano-channels with 200 µm × 200 µm patterned area, 0.8 µm channel width, and 0.7 µm spacer width takes ≈42 min (40 min alignment of EBL and 2 min exposure). The time for longer channels will only slightly increase the exposure time:, e.g., for a 200 µm × 400 µm channel pattern, it takes 44 min (40 min alignment and 4 min exposure).

Construction of Nanodevice: Before the graphite transfer, the nano-channel was immersed in Milli-Q water for 10 min to remove potentially water-soluble substances. The transfer of graphite from PDMS to the PMMA channel was performed using a 3D displacement platform in the glove box. The graphite sheets and nano-channels were aligned using a long-focus optical microscope. The 70–80 °C heating was adapted to improve the transfer rate. Note that PMMA was still solid at this temperature and the channel can retain its shape. Capping of the monolayer graphene was done by wetting transfer of CVD graphene onto the channel. The wetting transfer process was described in the literature.[12]

Topography Characterizations: The topography of the nanodevice was studied by scanning force microscopy (Dimension ICON FastScan, Bruker) in the peak force mode. The peak force was tuned for different experiments. Tapping mode was only used for the data in Figure S7 (Supporting Information). OTESPA probes (OPUS by MikroMasch, k = 26 N/m, f = 300 kHz) and Arrow-NC probe (NanoWorld AG, k = 42 N/m, f = 285 kHz) were used for the tapping mode, and the OLTESPA probes (OPUS by MikroMasch, k = 2 N/m, f = 70 kHz) for the peak force mode. The elasticity and deflection sensitivity of cantilevers were calibrated with the thermal tune method without contact. After the measurement, the images were processed in the NanoScope Analysis software. The sagging depth of each device was the average value of five measures.

SFM-IR Measurements: By combining SFM and infrared (IR) spectroscopy, SFM-IR record IR spectra and the chemical information and distribution with a nanometer spatial resolution. In the experiment, SD-NCHAu25-W probes (10–130 N m^{-1}, >320 kHz, Nanosensors, Switzerland) were applied to capture the spectroscopy data of nanodevices in the tapping mode. The spectrum on 12 nm thick PMMA spacer, clean nano-channel, graphene-covered nano-channel, and 9 nm graphite-covered nano-channel were investigated by SFM IR at 1730 cm^{-1}.

Supporting Information

Supporting Information is available from the Wiley Online Library or from the author.

Acknowledgements

The authors thank L. Gao at Max Planck Institute for Polymer Research for the help with graphite exfoliation. This research was supported by the German Research Foundation (SFB TRR 173 SPiN+X, A01+B02 #268565370) and the European Commission (Horizon Europe Project no. (101070290) NIMFEIA, and (101071937) n-AQUA. Min Liu thanks the China Scholarship Council (scholarship number 202106420057) for financial support.

Conflict of Interest

The authors declare no conflict of interest.

Data Availability Statement

The data that support the findings of this study are available from the corresponding author upon reasonable request.

Keywords

AFM-IR spectroscopy, nano-channels, nanofluidics, PMMA, sagging depth

Received: July 21, 2024
Revised: September 20, 2024
Published online:

[1] X. Liu, C. Sun, X. Ye, X. Zhu, C. Hu, H. Tan, S. He, M. Shao, R. W. Li, *Adv. Mater.* **2024**, *36*, 2311472.
[2] N. Yang, S. Yu, W. Zhang, H. Cheng, P. Simon, X. Jiang, *Adv. Mater.* **2022**, *34*, 2202380.
[3] H. Ma, X. Zhang, G. Feng, B. Ren, Z. Pan, Y. Shi, R. Xu, P. Wang, Y. Liu, G. Wang, *Sep. Purif. Technol.* **2023**, *312*, 123319.
[4] Y. Sun, C. Zhan, P. R. C. Kent, M. Naguib, Y. Gogotsi, D.-e. Jiang, *ACS Appl. Mater. Interfaces* **2019**, *12*, 763.
[5] A. Sugahara, Y. Ando, S. Kajiyama, K. Yazawa, K. Gotoh, M. Otani, M. Okubo, A. Yamada, *Nat. Commun.* **2019**, *10*, 850.
[6] C. Liu, X. Zou, Y. Lv, X. Liu, C. Ma, K. Li, Y. Liu, Y. Chai, L. Liao, J. He, *Nat. Nanotechnol.* **2024**, *19*, 448.
[7] R. Tunuguntla, F. Allen, K. Kim, A. Belliveau, A. Noy, *Biophys. J.* **2016**, *110*, 338A.
[8] P. Robin, T. Emmerich, A. Ismail, A. Niguès, Y. You, G. H. Nam, A. Keerthi, A. Siria, A. K. Geim, B. Radha, *Science* **2023**, *379*, 161.
[9] P. Robin, N. Kavokine, L. Bocquet, *Science* **2021**, *373*, 687.
[10] N. Kavokine, S. Marbach, A. Siria, L. Bocquet, *Nat. Nanotechnol.* **2019**, *14*, 573.
[11] L. Fumagalli, A. Esfandiar, R. Fabregas, S. Hu, P. Ares, A. Janardanan, Q. Yang, B. Radha, T. Taniguchi, K. Watanabe, G. Gomila, K. S. Novoselov, A. K. Geim, *Science* **2018**, *360*, 1339.
[12] Q. Yang, P. Z. Sun, L. Fumagalli, Y. V. Stebunov, S. J. Haigh, Z. W. Zhou, I. V. Grigorieva, F. C. Wang, A. K. Geim, *Nature* **2020**, *588*, 250.
[13] J. Li, D. Stein, C. McMullan, D. Branton, M. J. Aziz, J. A. Golovchenko, *Nature* **2001**, *412*, 166.
[14] S. A. Miners, G. A. Rance, A. N. Khlobystov, *Chem. Soc. Rev.* **2016**, *45*, 4727.
[15] B. Radha, A. Esfandiar, F. C. Wang, A. P. Rooney, K. Gopinadhan, A. Keerthi, A. Mishchenko, A. Janardanan, P. Blake, L. Fumagalli, *Nature* **2016**, *538*, 222.
[16] A. K. Geim, *Nano Lett.* **2021**, *21*, 6356.
[17] A. Keerthi, S. Goutham, Y. You, P. Iamprasertkun, R. A. W. Dryfe, A. K. Geim, B. Radha, *Nat. Commun.* **2021**, *12*, 3092.
[18] J. Wang, H. Zhou, S. Li, L. Wang, *Angew. Chem., Int. Ed.* **2023**, *62*, 202218321.
[19] Y. You, A. Ismail, G.-H. Nam, S. Goutham, A. Keerthi, B. Radha, *Annu. Rev. Mater. Res.* **2022**, *52*, 189.
[20] Q. Yang, *Acc. Mater. Res.* **2022**, *4*, 1.
[21] J. Zhang, W. Liu, J. Dai, K. Xiao, *Adv. Sci.* **2022**, *9*, 2200534.
[22] M. Liu, H. Guo, J. Luo, X. Gui, Y. Xing, Y. Cao, *Sep. Purif. Technol.* **2024**, *353*, 128474.
[23] M. A. Mohammad, T. Fito, J. Chen, S. Buswell, M. Aktary, S. K. Dew, M. Stepanova, *Lithography*, Intech Open Access Publisher, London **2010**, 293.
[24] C. Duan, W. Wang, Q. Xie, *Biomicrofluidics* **2013**, *7*, 026501.

[25] Y. Cui, H. Guo, X. Yan, W. Zhou, Q. Ye, C. Ying, Z. Liu, J. Tian, *Nano Lett.* **2023**, *23*, 5886.
[26] A. Castellanos-Gomez, V. Singh, H. S. J. van der Zant, G. A. Steele, *Ann. Phys.* **2015**, *527*, 27.
[27] C. Lee, X. Wei, J. W. Kysar, J. Hone, *Science* **2008**, *321*, 385.
[28] C. H. Tu, M. Steinhart, R. B., M. Kappl, H. J. Butt, G. Floudas, *Sci. Adv.* **2023**, *9*, eadg8865.
[29] A. Dazzi, C. B. Prater, *Chem. Rev.* **2017**, *117*, 5146.
[30] L. M. Johnson, L. Gao, C. W. Shields Iv, M. Smith, K. Efimenko, K. Cushing, J. Genzer, G. P. López, *J. Nanobiotechnol.* **2013**, *11*, 22.
[31] M. L. Hupfer, D. Blaschke, H. Schmidt, M. Presselt, *Langmuir* **2021**, *37*, 13255.
[32] M. R. Reddy, A. R. Subrahmanyam, M. M. Reddy, J. S. Kumar, V. Kamalaker, M. J. Reddy, *Mater. Today Proc.* **2016**, *3*, 3713.
[33] C. J. Shearer, A. D. Slattery, A. J. Stapleton, J. G. Shapter, C. T. Gibson, *Nanotechnology* **2016**, *27*, 125704.